ИНСТИТУТ ЯДЕРНОЙ ФИЗИКИ
им. Г.И. Будкера СО РАН

M.M. Karliner, N.V. Mityanina,
B.Z. Persov, V.P. Yakovlev

LHC BEAM SCREEN DESIGN ANALYSIS

BudkerINP 94-45

НОВОСИБИРСК

LHC Beam Screen Design Analysis

M.M. Karliner, N.V. Mityanina
B.Z. Persov, V.P. Yakovlev

Budker Institute for Nuclear Physics
630090 Novosibirsk-90, Russia

Abstract

The problems connected with the design of a beam screen for dipole magnets of proton collider LHC are discussed. In particular, we consider restrictions connected with possible beam screen deformations at quench, from one hand, and with beam dynamics and energy losses, from another hand.

The beam screen design variants with copper strips coating and everywhere copper coating were considered. Mechanical stresses and deformations at quench are analysed as well as beam screen heating. Symmetrical multibunch transverse oscillations were considered with respect to their resistive instability and transverse resistive impedance. Image currents ohmic losses were calculated with the account of anomalous skin effect at low temperatures.

A compromise variant is put forward for the operating temperature choice and copper coating thickness.

Contents

1. Introduction

One of principle functions of the beam screen is interception of synchrotronous radiation (0.4 W/m) and image current ohmic losses (0.35 W/m) at average current in one beam ~0.8 A and bunch length σ~10 cm, in order that this power was not dissipated in cold bore walls at the level of 1.8 K. The cold bore and beam screen cross section is shown in fig.1.

Because of its location in strong magnetic field, the beam screen is subjected to the action of ponderomotive forces due to eddy currents flowing at magnetic field switching-off. The beam screen must be designed to bear multiple magnetic field switchings-off without damages and residual deformations.

For retaining the mentioned low level of image current losses, the beam screen must have small surface impedance with the account of skin effect. For this purpose, it must be coated with copper layer. The ponderomotive forces at quench depend on thickness of this layer, because eddy currents are determined by small copper resistance. Stainless steel at low temperatures in strong magnetic field has specific resistance about 1000 (at maximal energy) - 2500 times (at injection energy) greater than copper.

An additional condition imposed on the beam screen is connected with ensuring collective stability of symmetrical multibunch transverse oscillations modes. For that, so called transverse impedance must not exceed given values [1]. This condition is ensured by copper coating.

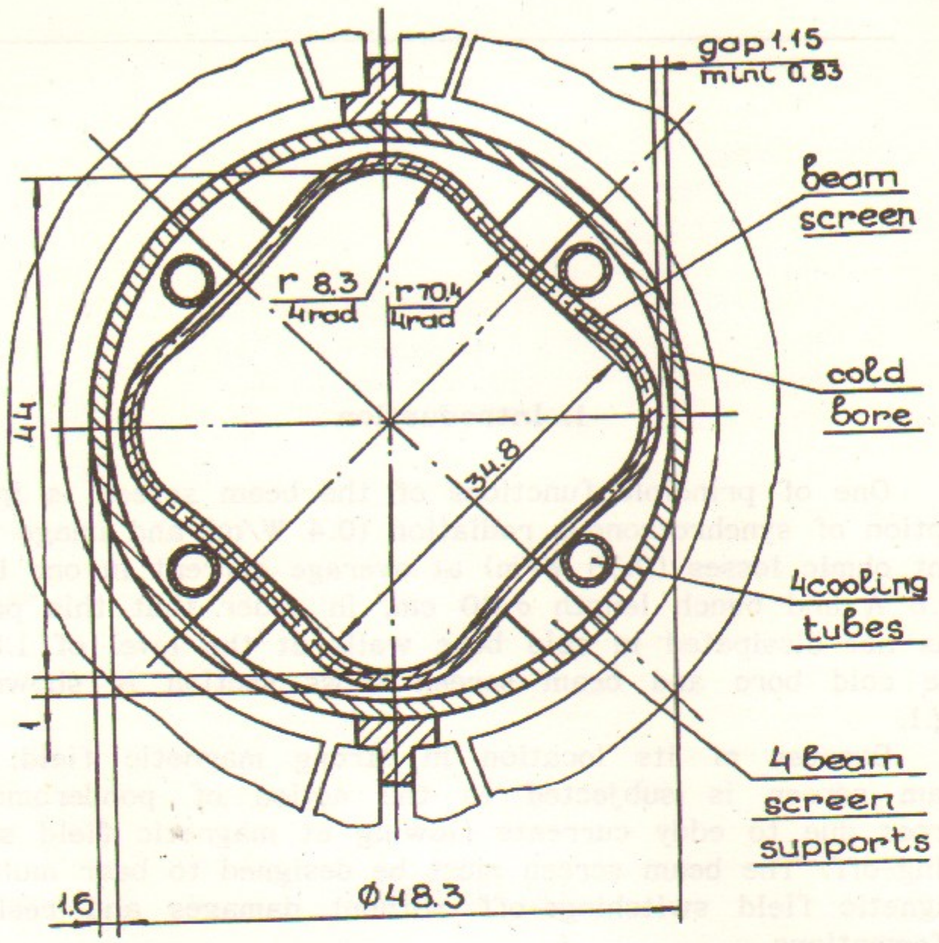

Fig. 1.

And finally, the operating temperature of the beam screen must be chosen in an optimal way. With a respect to thermodynamics, it is advantageously to take this temperature sufficiently high, for example, equal to the boiling point of liquid nitrogen. In this case copper resistance increases, which causes mechanical stresses and beam screen deformations at quench to decrease. But this can result in prohibitive increase of image current ohmic losses and also going transverse impedance over a given limit. Besides, at high beam screen temperature, absorption of heat by a cold

wall (liquid helium point ~ 1.8 K) can appear to be too big, which leads to big energy expenditure at compressor level. The beam screen temperature must be chosen in order to optimize, for example, total compressors power necessary for heat removal from the beam screen.

In order to satisfy contradicted requirements, it was suggested in [2] to make copper coating of four 18 mm wide strips. That causes mechanical forces to decrease, and transverse impedance growth is offered to compensate by the corresponding increase of copper coating thickness. Image currents were assumed here to flow in the main in copper strips with small resistance.

In order to have the possibility of optimal variant choice, we have made the calculations of beam screen electric parameters at various conditions. Operating temperatures 20 K, 50 K and 70 K were considered at the injection energy and maximal one. Calculations have been made for copper coating thickness 10, 20, 50, 100, 1000 2000 μm, stainless steel 1 mm, and besides, for everywhere copper coating and strips coating a half of a beam screen, as offered in [2]. For these conditions, image currents ohmic losses per unit length, transverse impedance and the instability growth rate for the most dangerous mode were calculated (see further).

Below, some explanations are given, in particular, the question of a dangerous frequency with respect to transverse oscillations stability (the frequency, for which one should to calculate transverse impedance and instability growth rate). According to criteria derived in [9] the frequency maximally contributing to the growth rate has a form $(k-Q)\cdot f_0>0$, where k is integer, Q is betatron tune, f_0 is revolution frequency. Because for LHC Q=70.3, the dangerous frequency is about 8 kHz (for k=71). In [1] and [2], another frequency was specified - 3.3 kHz (for k=70). But the latter frequency corresponds to damping a neighbour mode and therefore is not dangerous.

Transverse impedance was calculated assuming thickness of the stainless steel part of the beam screen to be much

more than skin depth, although in fact beam screen thickness is equal 1 mm, and skin depth for dangerous frequency 8 kHz is ~4 mm. On these grounds, it was assumed in [2] that image currents do not flow in beam screen parts without copper coating. But in fact the magnetic field penetrating through the beam screen meets a cold bore wall, also of stainless steel, with considerably greater thickness. As shown in App.2, a vacuum gap can be neglected at calculation, and total thickness of steel wall must be taken into account. Where the steel wall is coated with copper, almost the whole current flows in the copper layer, even if its thickness is less than skin depth in copper. Owing to this, transverse impedance at copper strips coating appears to be essentially greater than at everywhere coating.

Now, some words how to treat admittable value of transverse impedance. In our opinion, it must be done comparing growth rate caused by it with supposed decrement of a special feedback, which, as pointed in [1], should be present proceeding from other requirements: injection mistakes damping, emittance growth (because of vibrations and other factors) damping. The following values are pointed out: 1000 s^{-1} at injection energy and 500 s^{-1} at maximal energy. Caused growth rates should be with a reserve less than these values.

In the tables image current losses are given. At corresponding frequencies steel and copper thicknesses are much greater than skin depth. The losses are calculated summing those over all beam harmonics.

According to our calculations, everywhere copper coating is advisable. Its thickness can be essentially decreased (for example, 20 or 50 μm instead of 100 μm in [2]). It decreases noticeably quench forces and in the same time provides admittable transverse instability growth rate.

2. Electrodynamic parameters calculation

In this chapter we'll discuss the limitations for thickness of copper coating of the beam screen caused by the

multibunch transverse resistive instability. As there was mentioned above, the stainless steel beam screen wall has the thickness less than skin depth value for the frequency 8 kHz responsible for instability growth. As it shown in App.2, in this case the wall resistance will be close to one for the wall with infinite stainless steel wall coated (or not coated) by copper. Copper resistance depends both on the temperature and magnetic field. We use the next values for copper resistance ρ_c ($Ohm \cdot m \cdot 10^{10}$) for different beam screen wall temperature T and magnetic field B [2]:

	B = 0.0 Ts	B = 10.0 Ts
T = 20 K	1.55	6.16
T = 50 K	6.20	10.5
T = 70 K	15.0	19.1

The stainless steel resistance is $5 \cdot 10^{-7}$ Ohm·m. For our calculations we considered a round cross section of beam screen with the radius 18 mm. We used the next beam and storage ring parameters [3], [1]:

I =0.85 A - average beam current;
n_b=5940 - number of bunches in the beam;
s_b= 11 cm - bunch length [3];
E_1=0.45 TeV - injection energy;
E_2=7.7 TeV - maximal energy;
R = 4247 m - storage ring average radius;
n_x=70.3 - betatron frequency;
$\langle\beta_x\rangle$ = 82.5 m.

Below (tab.2.1) there are the results of calculations of maximal growth rate (GR) of multibunch transverse instability and of the beam screen wall transverse impedance (Rt) for frequency of 8 kHz for different values of copper coating thickness (DC). Calculations have been done both for beam injection energy and operating energy for total and for partial copper coating.

The growth rate values have been calculated according to App.1. Transverse impedance values have been calculated according to App.3.

Table 2.1

	everywhere coating		0.5 copper strips coating	
DC, mkm	GR., 1/s	Rt•<β>, GOhm	GR., 1/s	Rt•<β>, GOhm
	E=0.45 eV; T = 20 K			
10.00	46.65	12.17	197.22	51.51
20.00	24.24	6.32	186.01	48.59
50.00	10.10	2.64	178.94	46.75
100.00	6.22	1.63	177.01	46.24
200.00	6.57	1.72	177.18	46.29
500.00	6.59	1.72	177.19	46.29
1000.00	6.59	1.72	177.19	46.29
2000.00	6.59	1.72	177.19	46.29
	E=0.45 eV; T= 50 K			
10.00	37.25	35.79	242.52	63.32
20.00	78.70	20.53	213.24	55.69
50.00	34.27	8.94	191.03	49.90
100.00	18.03	4.71	182.91	47.78
200.00	11.64	3.04	179.72	46.95
500.00	12.50	3.27	180.15	47.06
1000.00	12.47	3.26	180.13	47.06
2000.00	12.47	3.26	180.13	47.06
	E = 0.45; T = 70 K			
10.00	31.16	60.27	289.48	75.56
20.00	54.73	40.35	251.26	65.61
50.00	75.21	19.62	211.50	55.24
100.00	40.43	10.55	194.11	50.71
200.00	22.23	5.81	185.01	48.33
500.00	18.74	4.90	183.27	47.88
1000.00	19.18	5.01	183.48	47.94
2000.00	19.18	5.01	183.49	47.94

Continuation Table 2.1

	E=7.7 TeV; T = 20 K			
10.00	7.77	34.68	14.05	62.77
20.00	4.43	19.78	12.38	55.32
50.00	1.92	8.59	11.12	49.73
100.00	1.01	4.52	10.67	47.69
200.00	.66	2.97	10.49	46.91
500.00	.71	3.20	10.52	47.03
1000.00	.71	3.19	10.52	47.02
2000.00	.71	3.19	10.52	47.02
	E = 7.7 TeV; T = 50 K			
10.00	11.11	49.56	15.72	70.21
20.00	6.89	30.75	13.61	60.80
50.00	3.16	14.11	11.74	52.48
100.00	1.67	7.46	11.00	49.16
200.00	.96	4.28	10.64	47.57
500.00	.93	4.16	10.63	47.51
1000.00	.93	4.16	10.63	47.51
2000.00	.93	4.16	10.63	47.51
	E= 7.7 TeV; T = 70 K			
10.00	14.89	66.41	17.61	78.64
20.00	10.50	46.84	15.41	68.85
50.00	5.34	23.85	12.83	57.35
100.00	2.92	13.02	11.62	51.94
200.00	1.59	7.09	10.96	48.98
500.00	1.20	5.37	10.76	48.12
1000.00	1.26	5.62	10.79	48.24
2000.00	1.26	5.62	10.79	48.24

Below (tab.2.2) there are results of calculations of the beam Ohmic losses per unit length (P/L) in the beam screen wall according to App.4:

The losses have been calculated using classical model of skin-effect, for anomalous skin effect (Chambers formulae, diffusion and full reflection models). One should see that the results for all three models are close. Wall losses for partial coating are more than ten times greater than for everywhere copper coating. Thus, copper strips coating looks to be unacceptable.

Table 2.2

		Power losse P/L, Wt/m:			
E, TeV	T, K	class. skin	anom. diff.	anom. refl.	0.5 copper strips
0.45	20	0.16	0.24	0.20	4.27
	50	0.30	0.33	0.30	4.34
	70	0.46	0.48	0.50	4.42
7.7	20	0.29	0.33	0.30	4.34
	50	0.38	0.40	0.39	4.38
	70	0.52	0.54	0.60	4.45

3. Mechanical and thermal problems at quench

3.1. Initial points

In this section, we analyse mechanical stresses and deformations of a beam screen and its heating by the quench currents. The analysis was carried out on the basis of the beam screen construction offered in [4] (fig.1)

At a superconductivity break-down ("quench") the magnetic field decreases rather quickly (according to [4] - within ~ 0.3 sec) from B_{max}=10 T to zero. The eddy currents induced in this time in the beam screen produce the ponderomotive forces, which deform the screen, tensing it in the horizontal direction and contracting - in the vertical one. According to [4], the screen must bear not less than 20 such cycles without mechanical damages and residual deformations.

We have considered here only variants with everywhere inner copper coating, because of shown above essential advantages of it in comparison with copper strips coating (for example, for 1/2 of the screen surface), in particular, with respect to the beam image current power losses.

The total heat release in the beam screen, according to [4], [1], [5], can be $q_0 \simeq .75$ W/m at average beam current 0.85 A in one beam and bunch length $\sigma \simeq 10$ cm. The synchrotron

radiation contribution is here ~0.4 W/m, and the beam image current ohmic losses are desired not to exceed ~0.35 W/m.

In order to decrease the latter parameter - the beam image currents losses, it is natural to decrease the electric resistance of screen inner coating. It can be achieved through the screen operating temperature lowering, because the copper specific resistance decreases in doing so. But that leads to increasing of eddy currents and, therefore, of mechanical stresses and screen deformations. Because of this, for the best solution choice, coatings of three thicknesses were analysed (20, 50 and 100 μm), made from copper of purity RRR100.

Besides, the change of the screen operating temperature is associated with the change of energy expenditure to evacuate the heat released in the screen to the zone with T=300 K. So, for example, at too high beam screen operating temperature, the heat evacuation is easier, but heat gain by the cold bore through radiation and supports heat conduction increases. And this heat must be evacuated already from the cold bore with the temperature T=1.8 K. With respect to that, an optimization of the screen operating temperature is possible for minimal energy expenses "at compressor level" [2]. This optimization is fulfilled further, but for more complete comprehension, the screen operation at quench was studied at three temperatures - 20, 50 and 70 K.

The inner copper coating presence gives rise to one more mechanical problem at quench - a problem of joint operation of steel screen shell and thin copper coating. The analysis shows that practically at any possible constructive and operating screen parameters mechanical stresses in copper coating can not be less than the elastic limit. Nevertheless, the screen must fulfil necessary number of quench cycles without mechanical damages.

An adequate solution of this problem seems us to be the following.

The copper layer shake-down, when working in the elastic-plastic region (i. e. at the stresses about the copper elastic limit or higher) is determined by the actual values of relative deformations of this layer. And this

deformation for the copper layer is established by the steel shell. Therefore this shell must work in the elastic region and at the stresses, when the relative deformation at the boundary "steel-copper" would possibly less.

Finally, it is necessary to estimate the influence on the screen operation at quench of the dynamic nature of the quench forces. A precise calculation of the corresponding plane bending oscillations mode eigen frequency for a mounted on supports screen with rather complicated cross section (fig.1) was not fulfilled; however, this frequency must be, in any case, higher than one for free steel round ring with the average radius 22.5 mm and a wall thickness 1 mm. And the estimation of the latter frequency by the method recommended in [6] gives 1200 ÷ 1300 Hz, when the characteristic frequencies of quench forces action lie within 1.5 ÷ 3 Hz (at the quench time 0.3 sec). On this basis, the forces acting on the screen during quench were treated by us as static ones.

The results obtained by the investigations of all mentioned questions are given further (the detailed calculations are given in App.5)

Besides considerable mechanical stresses and deformations, the currents induced in the screen at quench cause as well its essential heating. These processes are also considered further.

3.2. The optimal operating temperature

As mentioned above, the optimal operating temperature of the beam screen was determined for minimal energy expenditures at a removal of all heat released in the beam screen with the account of heat transfer to the cold bore.

A criterion was a parameter

$$k=k_1+k_2=q_k\frac{T_0-T_k}{T_k}+(q_0-q_k)\frac{T_0-T}{T},$$

where T_0=300 K, T_k=1.8 K, T is a beam screen temperature, q_0=0.75 W/m, q_k is a power transferred from the screen to the cold bore, W/m. Emissivity factor for the beam screen as well as for the cold bore was taken, as in [2], $\varepsilon\simeq 0.1$.

The results of calculations are given in tab.3.1:

Table 3.1

T,K	1.8	10	20	30	40	50	60	70	80
k_1	0	.38	.85	1.40	2.09	3.03	4.37	6.28	8.96
k_2	124.3	21.68	10.43	6.68	4.79	3.66	2.90	2.34	1.91
k	124.3	22.06	11.28	8.08	6.88	6.69	7.27	8.62	10.87

As it follows from the tab.3.1, with respect to the energy, the operating temperature 40÷50 K is optimal.

3.3. Mechanical stresses at quench

Fig.2 shows a sketch of a quater of a steel shell of the beam screen cross section. Copper coating is applied to the inner surface of this shell, therefore the mechanical stresses on this surface are of most interest. Maximal tension stresses on it take place in a section "*a-a*" (σ_a), maximal contraction stresses - in a section "*e-e*" (σ_e). According to A5.14 (App.5), these stresses can be calculated as

$$\sigma_a=\frac{6M_a}{t^2}+\frac{A_a}{t} \qquad (3.1)$$

$$\sigma_e=-\frac{6M_e}{t^2}, \qquad (3.2)$$

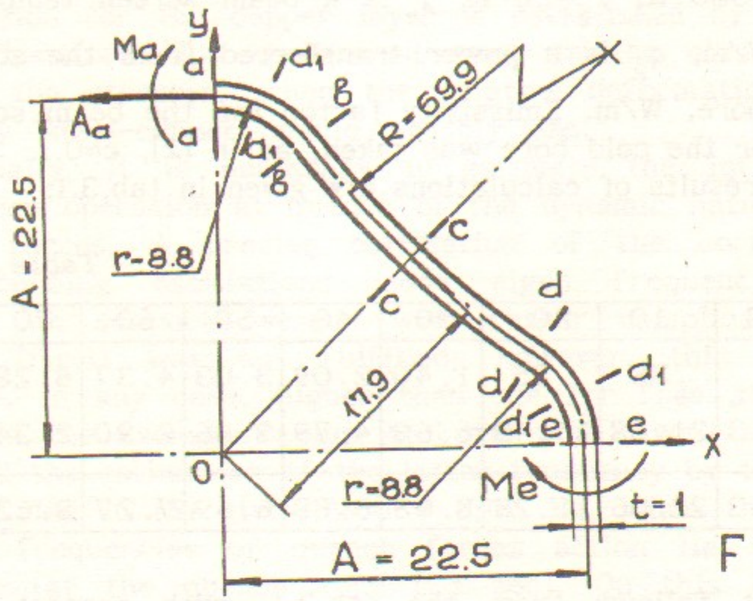

Fig. 2.

which gives, with the account of A5.12 and A5.13:

$$\sigma_a = \frac{6\cdot 43\cdot 10^{-3} Q_0}{10^{-6}} + \frac{5.436\cdot Q_0}{10^{-6}} \simeq .263 Q_0, \text{MPa} \simeq .0263 Q_0, d\text{aN/mm}^2, \quad (3.1')$$

$$\sigma_e = -\frac{6\cdot 30\cdot 10^{-3} Q_0}{10^{-6}} = -.18 Q_0, \text{MPa} = -.018\ Q_0,\ d\text{aN/mm}^2. \quad (3.2')$$

(In latter expressions Q_0 is measured in N/m.)

With the account of tab.A5.1 the stresses σ_a and σ_e become values given in tab.3.2.

Thus, for copper coating thickness Δ=100 μm at all considered temperatures, and for Δ=50 μm at the temperature 20 K, the stresses in the steel shell on the boundary "steel - copper" either exceed or are dangerously close to elastic limits of steels - possible variants of beam screen material (316LN, X20MD, 13RM19, a russian specification 12X18H10T and

Table 3.2

Δ, μm	Operating temperature, K					
	20		50		70	
	Stresses, daN/mm^2					
	σ_a	σ_e	σ_a	σ_e	σ_a	σ_e
20	31.7	-21.7	16.7	-11.4	9.2	-6.3
50	77.5	-52.9	39.6	-27.1	21.1	-14.4
100	153.6	-105	78	-53.2	40.8	-27.8

other). As acceptable variants, we can consider here the copper coating thickness 20 μm at all (20÷70 K) operating temperatures or the thickness 50 μm at the temperatures 50÷70 K.

A copper coating state can be analysed on the basis of a linearized joint steel and copper test diagram (for T=50÷70 K - fig.3). One can see that the stress in copper achieves elastic limit (~8÷9 daN/mm^2) already at the stress in steel > 12÷14 daN/mm^2. However, even at the stresses in steel near to its elastic limit (~40 daN/mm^2), the *total* relative deformation of steel (and hence, of copper on its surface) does not exceed 0.002 (0.2%). The *residual* relative deformation of copper, even in this case, does not exceed 0.13÷0.14%. It allows to hope that copper coating of the thickness 20÷50 μm at the operating temperature 50÷70 K will work reliably during required 20 quench cycles.

3.4. Beam screen deformations at quench

Maximal beam screen deformations by the quench forces action are changes in its horizontal and vertical transverse dimensions. These values, calculated by the method given in App.5, can be described as

$$\delta_x \simeq 5.89\cdot 10^{-7} Q_0, \text{m}, \quad (3.3)$$

$$\delta_y \simeq -5.94\cdot 10^{-7} Q_0, \text{m}, \quad (3.4)$$

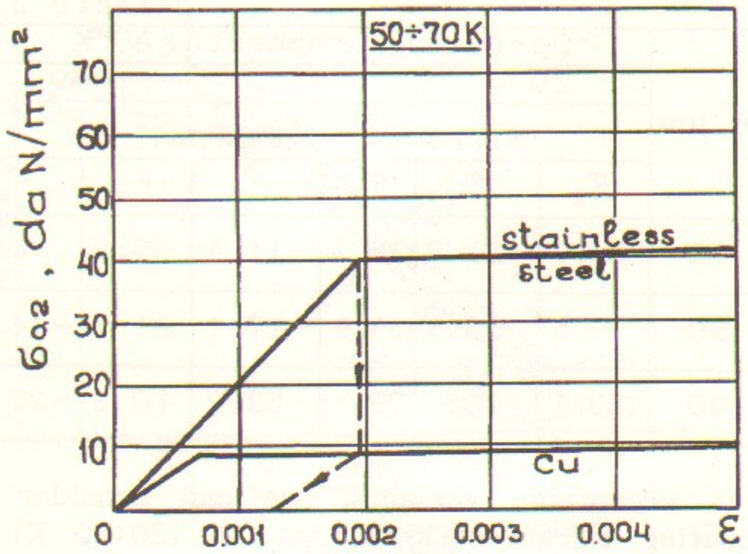

Fig. 3.

where δ_x and δ_y are total changes of horizontal and vertical transverse dimensions correspondingly; a sign "+" corresponds here to size increase, "-" - to size decrease.

Taking into account values Q_0 given in tab.A5.1, we get following beam screen deformation values depending on the operating temperature and copper coating thickness:

Table 3.3

Δ, μm	Operating temperature, K					
	0		50		70	
	Screen deformations, mm					
	δ_x	δ_y	δ_x	δ_y	δ_x	δ_y
20	.71	-.72	.37	-.38	.21	-.21
50	1.73	-1.75	.89	-.90	.47	-.48
100	3.44	-3.46	1.74	-1.76	.91	-.92

The tab.3.3 allows following important conclusions:

- at the nominal gap value between the beam screen and the cold bore 1.15 mm (fig.1) obtained deformation values at Δ=100 μm for temperatures 20÷50 K and at Δ=50 μm for a temperature 20 K are unacceptable;

- actual screen deformations can be somewhat (but not essentially, in our opinion) different from those given in tab.3.3, because of screen supports, which were not taken into account in the calculations;

- at the stresses corresponding to Δ=100 μm at all temperatures and to Δ=50 μm at T=20 K (tab.3.2), a dependence between deformation and stress becomes nonlinear, and as a result, actual values of deformations can far exceed (according to [7] - 10 times and more) those given in tab.3.3, based on the linear dependence.

Therefore, in this case also, the only actually possible combinations are Δ=20 μm at T=20÷70 K and Δ= 50 μm at T=50÷70 K.

3.5. Beam screen heating at quench

Currents, induced in the beam screen at quench, except dangerous stresses and deformations, produce its essential heating. Different screen sections are heated in the process differently, and one can show that no essential heat redistribution over a screen contour takes place during quench.

A time constant of temperature relaxation can be determined in this case as

$$\tau_c \simeq mcR_T, \text{ s}, \qquad (3.5)$$

where $m=\gamma_{ss} \cdot t \cdot l_{a1d1}$ is a unit length mass of the screen steel shell (neglecting the mass of a thin copper layer) on a region between sections a_1 and d_1 - fig.2 (here γ_{ss} is steel density, t is shell thickness, l_{a1d1} - is the length of the region between sections a_1 and d_1);

c is specific heat of beam screen steel;

$R_T = \frac{l_{a1d1}}{\lambda_f t}$ is heat resistance of the region l_{a1d1},

$\lambda_f \simeq \frac{\Delta\cdot\lambda_{Cu} + t\cdot\lambda_{ss}}{\Delta + t}$ is thermal conductivity factor for screen material (the thin copper layer, not changing essentially screen mass, nevertheless, increases considerably heat conduction) - here λ_{Cu} and λ_{ss} are thermal conductivities of copper and stainless steel correspondingly in the screen shell.

For example, at the operating temperature T=50 K $\lambda_{ss} \simeq 6.1$ W/(m·K), $\lambda_{Cu} \simeq 1100$ W/(m·K), and for $\Delta = 50\mu$m and t=1mm

$$\lambda_f = \frac{5\cdot10^{-5}\cdot1100 + 10^{-3}\cdot6.1}{5\cdot10^{-5} + 10^{-3}} \simeq 58 \text{ W/(m·K)} .$$

Then at $c \simeq 85$ J/(kg·K) and $\gamma_{ss} = 7850$ kg/m^3 a time constant of temperature relaxation becomes

$$\tau_c = mcR_T = \frac{c\gamma_{ss} l_{a1d1}^2}{\lambda_f} = \frac{85\cdot7850\cdot(2.5\cdot10^{-2})^2}{58} \simeq 7.2 \text{ s} ,$$

which far exceeds heating time (equal to quench time $\tau_0 \simeq .3$ s), and therefore, main heat redistribution over the screen contour takes place in a time interval about 20÷30 s. after quench finishing.

A temperature of arbitrary screen contour point after quench, as can be easily shown, can be found from relation:

$$T = T_0 + \Delta T = T_0 + \frac{\tau_0}{t\gamma_{ss} c}\left(\frac{t}{\rho_{ss}} + \frac{\Delta}{\rho_{Cu}}\right)\left(\frac{dB}{d\tau}\right)^2 x^2, \text{ K}, \qquad (3.6)$$

where x is the abscissa of the screen point in question. The temperatures of characteristic contour sections, calculated by relation (3.6), for different thicknesses of copper coating and operating temperatures are given in tab.3.4:

Table 3.4

Δ, μm	Section	Operatitg temperature, T_0		
		20	50	70
20	a_1	22.9	50.2	70.1
	c	34.9	52.4	70.8
	d_1	44.8	56.2	72.1
50	a_1	25.9	50.6	70.2
	c	42.9	55.3	71.7
	d_1	55.0	62.0	74.5
100	a_1	29.4	51.1	70.3
	c	50.3	59.0	73.1
	d_1	64.1	68.5	77.7

As seen from tab.3.4, an essential screen overheat during quench relative the operating temperature takes place for all coating thicknesses at operating temperature 20 K and at all operating temperatures for coating thickness 100 μm. Therefore, preferable parameters in this case are copper coating thickness 20÷50μm at operating temperatures 50÷70 K.

4. Conclusion

To summarize the conclusions made in sections 3.2÷3.5, it seems to be advantageous for a LHC beam screen at the cross section offered in [4] to accept the following main parameters:

- everywhere inner copper coating thickness - 20÷50 μm;
- operating temperature - 40÷50 K.

Appendix 1

Transverse oscillations resistive instability growth rates

In this section, we consider transverse oscillations growth rates for resistive instability in a round chamber with a multilayer wall (for the cases of everywhere coating and strip copper coating).

Resistive instability for a storage ring with a rectangular cross section was studied in [9] for a beam with arbitrary charges distribution.

The cross section geometry for our present problem differs essentially from the case considered in [9]; it is schematically shown in the fig.4a. It seems natural to use the model of a chamber with the round cross section of the same transverse dimension to study resistive instability now (fig.4b).

The second difference from [9] consists in the chamber walls surface impedance, which is not now uniform over a cross section circumference, because the steel chamber walls are covered with four symmetrically placed copper strips, which also are shown in the fig.4a,b. (The extreme cases are everywhere copper coating and no copper coating.)

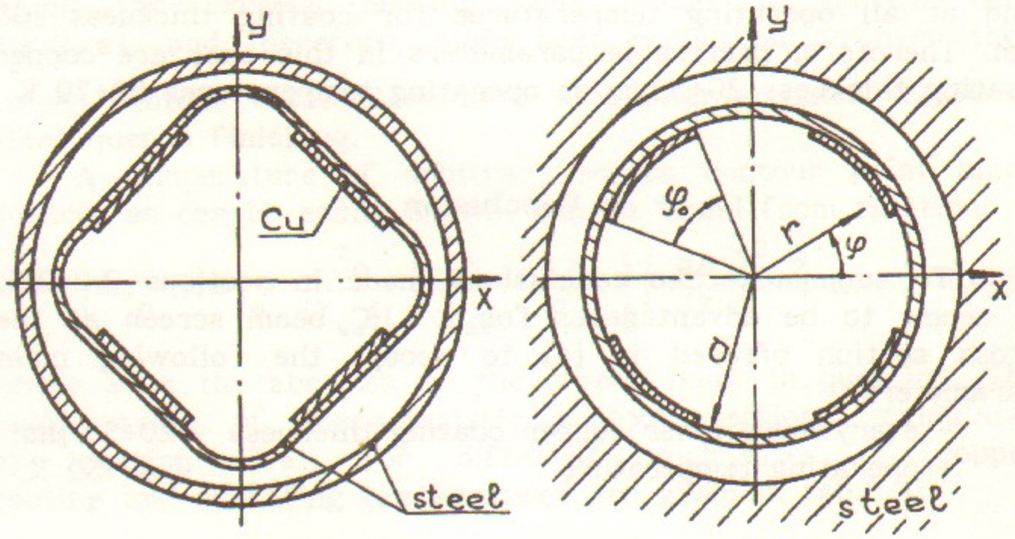

a) *Fig. 4,a,b.* б)

Moreover, projected steel and copper thicknesses are rather small and are comparable or even less than skin depth at minimal current spectrum frequency. Therefore, usual Leontovich boundary conditions (for the walls much more thick than skin depth) can be not quite correct now. This problem will be considered in App.2, and now it is sufficient for us to distinguish surface impedance of open steel regions and those with copper coating.

Further we will show that final expressions for growth rates, power losses and impedances contain surface impedance averaged over the chamber circumference. Therefore, as steel conductivity is about 1000 times less than copper one, the open steel regions give the main contribution into these values.

a. The electromagnetic field induced by the beam in the storage ring chamber with walls of finite conductivity

We will use now the same method as in [9], but for a chamber with circular cross section and for not uniform boundary conditions. In this paper, we will not give the detailed deduction of obtained results, but only brief account of the main differences from [9] and the final results.

We suppose that the conditions at copper/steel boundary change with a jump (neglecting the fact, that they change on a distance of order of skin depth). Notice that copper strips coating does not produce any image currents redistribution over the beam screen contour, as they are determined only by the beam magnetic field.

Following the perturbation theory, the field induced by the beam in the chamber is a sum of a field in an ideal waveguide $\mathbf{E}^0$ ($\mathbf{H}^0$) and an additional field arising due to the finite walls conductivity $\mathbf{E}_{add}$ ($\mathbf{H}_{add}$). The boundary conditions for fields Laplace transforms in the first approach become

$$\mathbf{E}_{add} \times \mathbf{n} = \xi(\varphi, s)\, \mathbf{H}^0, \qquad \text{(A1.1)}$$

where

$$\xi(\varphi,s)=\begin{cases}\xi_c(s) \text{ for } |\varphi-(\pi/4+k\pi/2)|\le\varphi_0/2,\\ \xi_s(s) \text{ for } \varphi_0/2\le|\varphi-(\pi/4+k\pi/2)|\le\pi/4,\ k=0,\dots,3,\end{cases} \tag{A1.2}$$

ξ_c and ξ_s describe the surface impedance of the wall covered with copper strips and of the open steel wall correspondingly (App.2); φ is the angular coordinate of the polar reference system used now for the chamber cross section; φ_0 is the angular dimension of four copper strips, symmetrically placed on the chamber walls (fig.4b); s is the Laplace variable, which will be further dropped for simplicity, except specially mentioned cases.

The additional fields can be spread over azimuthal harmonics which can be expressed via the membrane functions Φ_m and ψ_m (m is the azimuthal harmonic number), analogously to [9] (eqs.(7) - (9)). But substituting them into the boundary conditions (A1.1) we must take into account angular dependence of the surface impedance (A1.2).

For a round chamber of a radius a the waveguide eigen functions are

$$\phi_{kr}(r,\varphi)=A_{kr}J_k(\nu_{kr}r/a)e^{ik\varphi},\ J_k(\nu_{kr})=0,\ A_{kr}^2=1/(\nu_{kr}J'_k(\nu_{kr}))^2,$$

$$\psi_{kr}(r,\varphi)=A'_{kr}J_k(\nu'_{kr}r/a)e^{ik\varphi},\ J'_k(\nu'_{kr})=0,\ A'^2_{kr}=1/((\nu'^2_{kr}-k^2)J^2_k(\nu'_{kr})),$$

where

$$\int_0^a\left|\left[\begin{Bmatrix}g&\phi\\ g'&\psi\end{Bmatrix}_{kr}\right]^2\right|2\pi r\,dr=1,$$

$$g_{kr}=\nu_{kr}/a,\ g'_{kr}=\nu'_{kr}/a. \tag{A1.3}$$

The equations and boundary conditions for membrane functions have a form:

$$\Delta\begin{Bmatrix}\Phi\\ \Psi\end{Bmatrix}_m-\alpha_m^2\begin{Bmatrix}\Phi\\ \Psi\end{Bmatrix}_m=0; \tag{A1.4}$$

$$\Phi_m(r,\varphi)\Big|_{r=a}=-\frac{\xi(\varphi)}{4\pi R}A_m\sum_{k,r}\frac{\partial\phi_{kr}}{\partial r}J_{krm}\Big|_{r=a},$$

$$\frac{\partial}{\partial r}\Psi_m(r,\varphi)\Big|_{r=a}=-\frac{\xi(\varphi)}{4\pi R}A_m\sum_{k,r}\frac{\partial^2\phi_{kr}}{r\partial r\partial\varphi}J_{krm}\Big|_{r=a}, \tag{A1.5}$$

Here $\alpha_m^2=(m/R)^2+(s/c)^2$, $A_m=-im/(R\,\alpha_m)$ are functions of the Laplace variable s; R is the storage ring radius; J_{krm} is proportional to the beam current harmonic [9]:

$$J_{krm}=\frac{2\gamma_{kr}}{\gamma_{kr}^2+(m/R)^2}I_{krm}(s+im\omega_0),$$

$$\gamma_{kr}^2=g_{kr}^2+(s/c)^2.$$

For a symmetrical beam consisting of n_0 equal bunches the current density (neglecting longitudinal synchrotron oscillations) is

$$j_z(x,y,z,t)=2\pi R\ I/n_0\sum_{n=1}^{n_0}\delta(z-R\theta_n)\delta(r_\perp-r_{\perp n}(t)),\ \theta_n=2\pi n/n_0,$$

$$z=l-\omega_0 Rt, \tag{A1.6}$$

l - longitudinal coordinate, ω_0 - revolution frequency, I - averaged beam current, $r_{\perp n}$ - n-th bunch transverse position in the polar system (r,φ): $r_{\perp n}=(r_n,\ \varphi_n)$; it depends on the time because of betatron oscillations; for vertical oscillations $\varphi_n=0$.

The current harmonic, according to [9], is

$$I_{krm}(s+im\omega_0)=-2\pi R\ I/n_0\ \frac{g_{kr}^2}{\gamma_{kr}}A_{kr}\ \times$$

$$\times\sum_{n=1}^{n_0}\exp(-im\theta_n)L\left(\exp(ik\varphi_n)J_k(g_{kr}r_n)\right). \qquad (A1.7)$$

Searching the solution of eq.(A1.4) in a form

$$\begin{Bmatrix}\Phi\\ \Psi\end{Bmatrix}_m=\sum_k\begin{Bmatrix}a\\ a'\end{Bmatrix}_{lm}\exp(il\varphi)\ I_l(\alpha_m r), \qquad (A1.8)$$

we get the coefficients a_{lm}, a'_{lm} from the boundary conditions (A1.5) as

$$\begin{Bmatrix}a\\ a'\end{Bmatrix}_{lm}=-\frac{A_m}{4\pi R\ \sqrt{\pi}a}\left[\begin{Bmatrix}I_l(\alpha_m a)\\ I'_l(\alpha_m a)\alpha_m a\end{Bmatrix}\right]^{-1}\sum_{k,r}\hat{\xi}(k-l)\ J_{krm}\begin{Bmatrix}1\\ ik\end{Bmatrix}, \qquad (A1.9)$$

where

$$\hat{\xi}(k-l)=\frac{1}{2\pi}\int_0^{2\pi}\xi(\varphi)\exp(i(k-l)\varphi)\ d\varphi, \qquad (A1.10)$$

$$\hat{\xi}(0)=\langle\xi\rangle=\frac{1}{2\pi}\int_0^{2\pi}\xi(\varphi)\ d\varphi$$

Thus, the membrane functions can be determined and the additional fields due to the resistivity can be found.

b. The transverse force

The transverse force m-th azimuthal harmonic can be written as ([9],(8))

$$F_{rm}=e(E_r-vB_\varphi)=-e\left(\frac{(im\omega_0+s\beta^2)}{im\omega_0}\frac{\partial\phi_m}{\partial r}+\frac{(s+im\omega_0)}{s}\frac{\partial\Psi_m}{r\partial\varphi}\right). \qquad (A1.11)$$

Turning formally to the reference system of equilibrium particle ([10], [9]) for ultrarelativistic beam ($\beta=v/c=1$) we

change the arguments of all functions depending on s in (A1.11): $s\to s-im\omega$ and get:

$$F_{rm}=-e\left(\frac{s}{im\omega_0}\frac{\partial\phi_m}{\partial r}+\frac{s}{s-im\omega_0}\frac{\partial\Psi_m}{r\partial\varphi}\right). \qquad (A1.12)$$

The coefficients a_{km}, a'_{km} for Φ_m, Ψ_m contain the beam current harmonic $I_{krm}(s)$, which for a beam with zero transverse size has a form:

$$I_{krm}(s)=-2\pi RI/n_0\sum_n\exp(-im\theta_n)L\left[L^{-1}\left[g_{kr}^2/\gamma_{kr}\right]\phi_{kr}(r_n,0)\right], \qquad (A1.13)$$

where r_n depends on the time because of betatron oscillations. In a linear approach, for small oscillations amplitudes, this time dependence is harmonic:

$$r_n(t)=r_{0n}\sin(\Omega t+\psi_n),$$

where Ω is the betatron frequency ($\Omega=\nu\omega_0$) and ψ_n is the phase shift for n-th bunch, for a given oscillation mode. The approach of small amplitudes gives also that only terms with $k=\pm1$ must be taken into account. Linearizing these terms, we get the opportunity to introduce the sin-dependent on the time function $\phi_{kr}(r_n,0)$ under the operator of inverse Laplace transform, thus L and L^{-1} in (A1.13) abolish one another.

But after this linearizing the series for a_{km}, a'_{km} become divergent if we neglect the beam transverse size σ. But we can take it into account, for example, in a simplest way

$$\delta(y-y_0)\to f(y)=\begin{cases}1/\sigma, & |y-y_0|\le\sigma/2,\\ 0 & |y-y_0|>\sigma/2,\end{cases}$$

and get that the beam current harmonic I_{krm} (for $k=\pm1$,

$\sigma \gg y_0$), instead of

$$\phi_{1r}(r_n,0) \approx A_{1r} r_n g_{1r}/2, \qquad \text{(A1.14)}$$

contains its averaged over the beam cross section value

$$\langle\phi_{1r}(r_n,0)\rangle \approx A_{1r}\left[J_1(g_{1r}\sigma/2)/(g_{1r}\sigma/2)\right] r_n g_{1r}. \qquad \text{(A1.15)}$$

Here the term in square brackets gives convergence of the series over the subscript r with a sum not depending on σ, and the time dependent r_n is contained in a linear way, which also leads to abolishing $\mathbf{L}$ and $\mathbf{L}^{-1}$.

Finally, we can write the transverse force m-th harmonic (in the reference system of the equilibrium particle [9]) as

$$F_{rm}(r,\varphi)=eI/n_0\ 2\pi R\,\frac{A_m}{4\pi R}\,\frac{1}{\pi a^3}\sum_{k,\pm}\hat{\xi}(\pm 1-k)\exp(ik\varphi)\sum_n \exp(-im\theta_n)\times$$

$$\times\frac{r_{0n}}{2i}\left(\frac{\exp(i\psi_n)}{(s-i\Omega)}-\frac{\exp(-i\psi_n)}{(s+i\Omega)}\right)\times$$

$$\times\left(\frac{s}{im\omega_0}\,\frac{I_k'(\alpha_m r)\alpha_m a}{I_k(\alpha_m a)}\mp\frac{s}{s-im\omega_0}\,\frac{I_k(\alpha_m r)}{I_k'(\alpha_m a)\alpha_m r}\right), \qquad \text{(A1.16)}$$

and the full force is

$$F_r(r,\varphi)=\sum_m F_{rm}(r,\varphi)\exp(imz). \qquad \text{(A1.17)}$$

c. Equations of the transverse motion and growth rates

The equations of vertical motion ([9], (18)) in the reference system of the equilibrium particle, in the variables action - phase, have a form:

$$\dot{J}_y = 2\sigma_y J_y = \overline{F_y\cdot(\partial y/\partial\psi_y)}\ ;\quad \dot{\psi}_y=\Omega+\overline{F_y\cdot(\partial y/\partial J_y)}\ ; \qquad \text{(A1.18)}$$

$$y=\sqrt{2J_y/(m_s\Omega)}\sin(\psi_y),\quad \dot{y}=\Omega\sqrt{2J_y/(m_s\Omega)}\cos(\psi_y),$$

where the line over the right hand sides denotes averaging over the time.

Writing the motion equations for beam bunches, we must calculate the force azimuthal harmonics (A1.16) at their transverse coordinates (small comparable with chamber radius). Moreover, returning to the definition of α_m, we can see that after the substitution $s \to s-im\omega_0$ for the ultrarelativistic particles $\alpha_m \to 0$. These two reasons lead to the result that (A1.16) contains the nonzero terms only with $k=\pm 1$.

Thus, after averaging over the time, the first equation of (A1.18) for a bunch with a number p, according to [9] (for vertical oscillations $F_y=F_r$), we get:

$$\dot{J}_{yp}=-\omega_0\,\frac{I/n_0}{V_s\nu\,4\pi}\left(\frac{R}{a}\right)^3\sum_{m,n,\pm}\pm\hat{\xi}_m^{\pm}(0)\frac{\exp(im(\theta_p-\theta_n)\pm i(\psi_p-\psi_n))}{m\pm\nu}J_{yn}, \qquad \text{(A1.19)}$$

where

$$\hat{\xi}_m^{\pm}(0)=\hat{\xi}(0)\Big|_{s=-(im\omega_0\pm i\Omega)}=\langle\xi(-(im\omega_0\pm i\Omega))\rangle=$$

$$=(\xi_s+(\xi_c-\xi_s)2\varphi_0/\pi)\Big|_{s=-(im\omega_0\pm i\Omega)}, \qquad \text{(A1.20)}$$

the brackets $\langle\rangle$ denote averaging over the chamber circumference.

Analogously one can write the second equation of (A1.18), for betatron phases of bunches and to find the growth rates for a beam with arbitrary charges of separate bunches, as in [9]. But here we will consider the normal oscillation modes of a symmetrical beam with equal charges of all bunches. For such modes all the amplitudes of bunches oscillations are equal and the phase shifts between bunches are determined from the symmetry condition.

Finally, for a mode with phase shift between neighbour

bunches $2\pi l/n_0$ ($l=0,\dots,n_0$) the growth rate is

$$\sigma_y^l = -\frac{4}{\pi}\,\omega_0\,\frac{I}{V_s\nu_y}\left(\frac{R}{2a}\right)^3 \mathrm{Re}\left\{\sum_{p=-\infty}^{\infty}\frac{\langle\xi(-(i(pn_0+l)\omega_0\pm i\Omega))\rangle}{pn_0+l+\nu_y}\right\}. \qquad \text{(A1.21)}$$

The transverse resistive impedance for the chamber with the circular cross section is given in App.3 ((A3.2)). As it is measured in Ohm/m, It can be multiplied, for convenience, by the machine beta function $\beta=2\pi R/\nu_y$:

$$Z_{t\beta}(\omega)= Z_t\,2\pi R/\nu_y = \langle\xi(-i\omega)\rangle\,4\pi(R/a)^3/(\omega R/c).$$

Thus the growth rate can be written as

$$\sigma_y^l = -\frac{1}{8\pi^2}\,\omega_0\,\frac{I}{V_s}\,\mathrm{Re}\left\{\sum_{p=-\infty}^{\infty}\langle Z_{t\beta}((pn_0+l)\omega_0\pm i\Omega)\rangle\right\}. \qquad \text{(A1.22)}$$

Note that in this form the expression for the growth rate has a general form, not depending on the chamber cross section form, which determines only the transverse impedance.

d. The comparison of the rectangular and circular cross sections

In [9], the resistive instability was considered for a rectangular chamber. It is natural that our present result must be near to the results of [9] for a square cross section of the same dimension.

The growth rates of normal modes in a chamber with the rectangular cross section a × b are ([9], (32)):

$$\sigma_y^l = -2\,\omega_0\,\frac{I}{V_s\nu_y}\,\frac{R^3}{(ab)^{3/2}}\,F(b/a)\sum_{p=-\infty}^{\infty}\frac{\xi(-(i(pn_0+l)\omega_0\pm i\Omega))}{pn_0+l+\nu_y},$$

$$\frac{1}{\sqrt{ab}}\,F\left(\frac{b}{a}\right)=\frac{1}{b}\sum_{k=0}^{\infty}\left\{\sin\left(\frac{k\pi}{2}\right)\frac{\frac{k\pi b}{2a}}{\mathrm{sh}\left(\frac{k\pi b}{2a}\right)}\right\}^2+\frac{1}{a}\sum_{k=0}^{\infty}\left\{\cos\left(\frac{k\pi}{2}\right)\frac{\frac{k\pi a}{2b}}{\mathrm{ch}\left(\frac{k\pi a}{2b}\right)}\right\}^2,$$

$$F(1)=0.474. \qquad \text{(A1.23)}$$

Comparing (A1.21) and (A1.23) we can see that the growth rates coincide for a square chamber with a wall lengths b and a round chamber with a diameter d if

$$d/b=(2/(\pi F(1))^{1/3}\approx 1.103,$$

i. e. the difference of chambers dimensions is about 0.1, rather small, which corresponds to our expectations.

Appendix 2

Surface impedance and boundary conditions for a multilayer wall

When calculating the electromagnetic field in the chamber with not ideal walls, the finite resistivity is usually taken into account in a form of Leontovich boundary conditions:

$$\mathbf{E}\times\mathbf{n} = \xi\,[\mathbf{H}\times\mathbf{n}]\times\mathbf{n}, \qquad \text{(A2.1)}$$

where $\xi(s)$ is the surface impedance, $\mathbf{n}$ is the outer normal to the surface, $\mathbf{E}(s)$ and $\mathbf{H}(s)$ are Laplace transforms of electric and magnetic fields. For wave normal incidence on the wall of infinite thickness

$$\xi(s)=Z_0\sqrt{\mu/\varepsilon(s)}=\sqrt{s\mu/\sigma} = Z_0\sqrt{s/(Z_0\sigma c)}, \qquad \text{(A2.2)}$$

$Z_0=\sqrt{\mu_0/\varepsilon_0}$ - the free space impedance, σ - the metal conductivity, ε and μ are relative electric (complex, depending on frequency for metals) and magnetic permiabilities correspondingly.

But our problem differs essentially from this model:

1) the wave in the chamber is propagating together with the beam, not normally, but along the wall, with the beam's phase velocity;
2) the wall consists of several layers of different conductivities and thicknesses comparable or even less then the skin depth .

Thus, the surface impedance should be modified to describe correctly our problem.

The most common case considered now is shown on the fig.5: the chamber wall consists of two layers (copper and steel), a vacuum gap separates the outer side of the wall from the surrounding screen of infinite thickness (which can have ε(s)=1, in the case of absence of this screen).

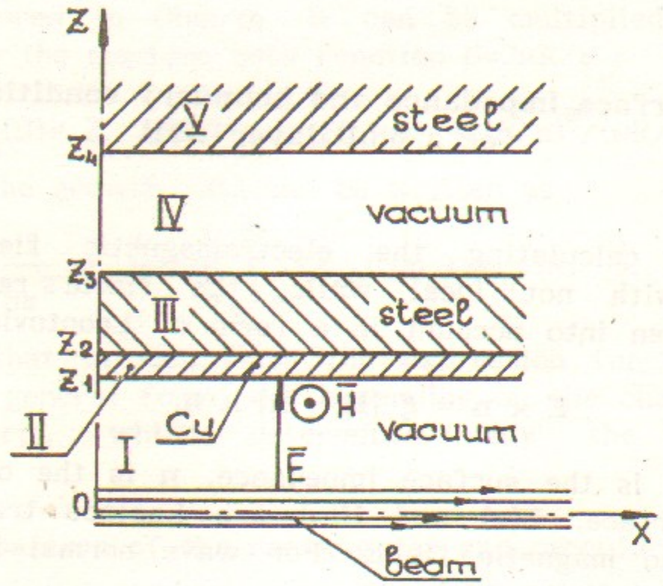

Fig. 5.

Further we assume that in all regions $\mu=1$ and denote

$$w_i = \sqrt{\mu/\varepsilon_i} = \sqrt{1/\varepsilon_i} = \sqrt{s/(Z_0\sigma_i c)}. \qquad (A2.3)$$

Consider a wave incidence on the metal surface, with an angle α_0 to its normal. The case of a longitudinal propagation corresponds to $\alpha_0=\pi/2$. For a nonideal wall $\alpha_0<\pi/2$ because the losses in the wall material mean the nonzero Poynting vector component normal to the surface and hence the nonzero corresponding wave vector component.

The sum of incident and reflected waves in every region can be written as

$$H_i=(H'_i\exp(ik_{zi}(z-z_i))+H''_i\exp(-ik_{zi}(z-z_i)))\exp(ik_{xi}x),$$

$$E_i=(E'_i\exp(ik_{zi}(z-z_i))+E''_i\exp(-ik_{zi}(z-z_i)))\exp(ik_{xi}x).$$

Amplitudes of incident and reflected waves are determined from the condition of tangential electric and magnetic fields components persistence at the boundary. Fields matching along the boundary at arbitrary x coordinate requires equal phase velocity x-components and results in

$$k_{xi}=k_{x0}=k_0\sin(\alpha_0),\ k_{zi}=k_0/w_i\sqrt{1-(w_i\sin(\alpha_0))^2}.$$

Wave vector components being found, tangential fields components matching condition, together with the connection of electric and magnetic fields components normal to the wave vector, allow to get all waves amplitudes in terms of incident wave, for example.

For metals usually $|w_1|\ll 1$, hence $|k_{zi}|\gg|k_{xi}|$. It means that for any angle of incidence α_0 the wave in the metal is propagating practically normally to the surface. In the vacuum gap the angle of the wave propagation must be equal α_0.

Therefore, in the case of longitudinal wave propagation the wave turns in the metal for an angle $\pi/2$, and further in the vacuum gap turns backward for $-\pi/2$. (In the case of normal wave incidence the wave direction remains normal).

The Maxwell equations give the connection between electric and magnetic fields components normal to the wave vector direction and to each other:

$$w_i E_{\perp i}=H_{\perp i}.$$

We consider here the incident wave with $H_y\neq 0$, $H_x=0$. In the regions with the normal wave propagation this equation connects H_y and E_x components, both tangential to the surface, whereas in the regions with the longitudinal wave propagation it connects H_y and E_z components, the tangential

to the surface component of the magnetic field and normal to the surface component of the electric field.

Matching the tangential components of the magnetic and electric field on all regions boundaries; denoting $\varphi_2=ik_{z2}d_2$, $\varphi_3=ik_{z3}d_3$ (phase shifts in z direction for second (copper) and third (steel) regions); taking into account that in the last region there is no reflected wave - we can write the system of conditions of fields tangential components matching on the regions boundaries.

The surface impedance ξ describes the ratio of tangential components of electric and magnetic field on the boundary of the first region:

$$\xi=E_{t1}(z_1)/H_{t1}(z_1)=E_{t2}(z_1)/H_{t2}(z_1). \qquad (A2.4)$$

Solving the system of boundary conditions, we get:

$$\xi=-Z_0w_2\frac{1+th(\varphi_2)\cdot\beta}{th(\varphi_2)+\beta},\quad \beta=\frac{w_2}{w_3}\cdot\frac{1-th(\varphi_3)\left(w_5\cos(\alpha_5)/w_3\right)}{th(\varphi_3)-\left(w_5\cos(\alpha_5)/w_3\right)}, \qquad (A2.5)$$

where α_5 describes the direction of the wave propagation in the last region : $\alpha_5\approx0$ for external metal wall of infinite thickness and $\alpha_5\approx\pi/2$ for infinite free space, without the outer wall).

Let's make some remarks to (A2.5).

1. It can be easily seen that if we take into account outer steel surrounding (region V with $w_5=w_3$), it is equivalent to the case of continuous steel wall of infinite thickness. It means that the gap between the wall and outer surrounding "is not seen" by the wave propagating along the wall. In this case for two layer wall

$$\xi=-Z_0w_2\frac{1-th(\varphi_2)\cdot w_2/w_3}{th(\varphi_2)-w_2/w_3} \qquad (A2.6)$$

and for one layer wall ($\varphi_2=0$), naturally,

$$\xi=Z_0w_3. \qquad (A2.7)$$

2. The case of the thin wall without outer surrounding differs essentially from one considered above. This case corresponds to $\beta=w_2/(w_3th(\varphi_3))$,

$$\xi=-Z_0w_2\frac{1+th(\varphi_2)\cdot w_2/(w_3th(\varphi_3))}{th(\varphi_2)+w_2/(w_3th(\varphi_3))}=-Z_0w_2\frac{w_3th(\varphi_3)+w_2th(\varphi_2)}{w_3th(\varphi_3)th(\varphi_2)+w_2}. \qquad (A2.8)$$

For the steel wall without copper coating

$$\xi=-Z_0w_3th(\varphi_3), \qquad (A2.9)$$

For the wall with thickness d_3 much less than skin depth $\delta=1/Re(k_{z3})$, as it is in our case ($\varphi_3\ll1$),

$$\xi\approx-Z_0w_3(\varphi_3-\varphi_3^3/3)=Z_0(-ik_0d_3+(k_0d_3)^3Z_0\sigma/3k_0),$$

$$Re(\xi)=Z_0^2\sigma\,k_0^2d_3^3/3. \qquad (A2.10)$$

The ohmic losses, proportional to $Re(\xi)$, are in this case much less than if we take into account outer surrounding. That can be seen if we compare image currents for these two cases.

The magnetic field inside the steel wall without outer steel surrounding is

$$H_1=H_0ch(ik_{z3}(z-z_3))/ch(ik_{z3}(z_2-z_3)),$$

and in the case of infinite steel wall (equivalent to the case with outer steel surrounding)

$$H_2=H_0exp(ik_{z3}(z-z_2)),$$

where H_0 is the magnetic field on the inner steel surface.

At our parameters (d_3~1 mm, $|1/\mathrm{Re}(k_{z3})|$~4 mm for frequency ~8 kHz), it leads to the fact that the full current flowing in steel in the first case makes up only about 0.03 of that for the second case, when surrounding is taken into account:

$$I_2 \sim H_0;$$
$$I_1 \sim H_0 |d_3 k_{z3}|^2/2 \approx 0.03\, I_2. \qquad \text{(A2.11)}$$

The currents difference results in the losses analogous difference.

3. Considering, for a comparison, a case of normal incidence of the wave on the two layer wall (without outer surrounding), one can get:

$$\xi = -Z_0 w_2 \frac{1 + \mathrm{th}(\varphi_2)\cdot\beta}{\mathrm{th}(\varphi_2)+\beta}, \quad \beta = \frac{w_2}{w_3}\cdot\frac{w_3 - \mathrm{th}(\varphi_3)}{w_3 \mathrm{th}(\varphi_3) - 1}. \qquad \text{(A2.12)}$$

For a thick outer layer ($\mathrm{th}(\varphi_3)=-1$) the surface impedance for normal wave incidence is the same as for the wave propagating along the wall, (A2.6). But for the thin wall without outer surrounding or for a screen of a material not identical with the wall outer metal ($w_5 \neq w_3$), the results for normal and tangential incidence are not the same.

For numerical calculations we used the expression (A2.6), corresponding to the two layer wall with outer screen of infinite thickness.

Appendix 3

Transverse resistive impedance of the round chamber

The transverse resistive impedance can be calculated in two ways: from the dipole longitudinal impedance, via the Panoffski-Wenzel theorem, or averaging the change of the transverse momentum because of the additional transverse fields due to walls resistivity (App.2).

Calculating the dipole longitudinal resistive impedance Z_{11}, we consider, following [11], a round beam of a current I in a round chamber of a radius a with walls surface impedance depending on the angle $\xi(\varphi)$:

$$\xi(\varphi) = \begin{cases} \xi_c & \text{for } |\varphi - (\pi/4 + k\pi/2)| \le \varphi_0/2, \\ \xi_s & \text{for } \varphi_0/2 \le |\varphi - (\pi/4 + k\pi/2)| \le \pi/4, \ k=0,\ldots,3. \end{cases}$$

The beam center is shifted relatively the chamber center on the small value x, which leads to the surface wall current density dipole deviation:

$$J = \frac{x\, I}{\pi a^2}\cos(\varphi).$$

The tangential magnetic field near the wall is equal to the surface current density J. Thus, integrating the losses in the chamber wall due to the finite conductivity, we get that it is expressed via the averaged over the chamber circumference surface impedance:

$$P_1 = Z_{11} I^2/2 = \int \xi(\varphi) H_\varphi^2(a,\varphi)/2\ a\ d\varphi = \frac{I^2 x^2}{2\pi\, a^3} \langle\xi\rangle, \qquad \text{(A3.1)}$$

where P is the resistive losses power for unit length, Z_{11} is the longitudinal dipole resistive impedance for unit length.

From the Panoffsky-Wenzel theorem the transverse resistive impedance for unit length is

$$Z_{t1} = Z_{11}/(kx^2),$$

thus, for the chamber length $2\pi R$

$$Z_t = Z_{t1} 2\pi R = \frac{\langle\xi\rangle}{a^3 k} 2R. \qquad \text{(A3.2)}$$

The transverse impedance can be calculated via the transverse momentum change for one turn for a beam current

harmonic $I_m \exp(-ik(l-vt))$, with a shift x relatively the chamber center. Integrating the transverse force (A1.11) over the storage ring circumference for such current instead of azimuthal harmonics, and dividing it by the beam current and shift x, we can get the same result (A3.2).

Appendix 4

Power losses due to walls resistivity, with the account of the anomalous skin-effect

The power losses due to the walls resistivity can be calculated

$$P = \frac{1}{2}\int [E \times H_0^*]_n \, dS = \frac{2I^2}{\pi a} \sum_{p>0} \langle \xi_r(-ipn_0\omega_0) \rangle \exp(-(pn_0\sigma_b/R)^2),$$

where I is the beam average current; n_0 is the number of bunches in the beam; ω_0 is the revolution frequency;a is the chamber cross section radius; σ_b is the bunch length; R is the storage ring averaged radius; $\langle \xi_r(-i\omega) \rangle$ is the real part of the surface impedance (averaged over the chamber cross section circumference).

We suppose here, as in App.1, that the conditions at copper/steel boundary change with a jump. It is valid because even for steel at lowest frequency $n_0\omega_0 \sim 60$ MHz skin depth is about 20 μm, much less than the curvature radius.

Calculating the power losses, we must sum up the terms up to the frequency about $\omega_{max} \sim \omega_0 R/\sigma_b$. At low temperatures the skin depth at such frequencies becomes comparable or even less than the electron free length, and the classical model of the skin-effect is not valid. (It does not concern the growth rates calculation because not the high frequencies, but the lowest ones give the main contribution there.) We have taken into account the anomalous skin-effect

following to the model and interpolation formulas of Pippard and Chambers ([12], [13]) for copper surface impedance.

The results of losses calculations show that the classical model gives smaller losses than the Chambers one.

Appendix 5

Beam screen mechanical stresses and deformations analysis

A magnetic flux for unit beam screen length through a zone of width $2x$ (fig.6) is

$$\Phi = 2x \cdot B, \qquad \text{(A5.1)}$$

and thus, a voltage induced at this screen region at quench becomes

$$U = -\frac{d\Phi}{d\tau} = -2x\frac{dB}{d\tau}. \qquad \text{(A5.2)}$$

Because the longitudinal conductivity of a turn, consisting of two regions ds of unit length, which are symmetrically placed relative the axis y, can be written as

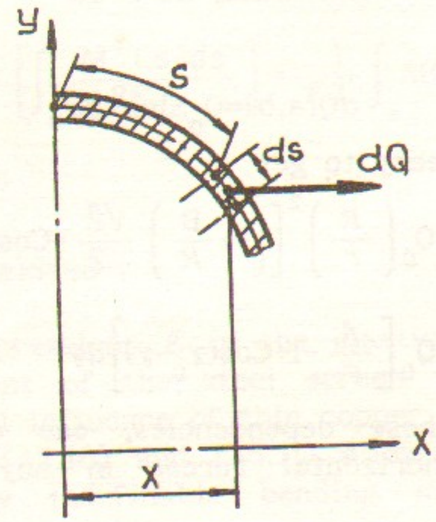

Fig. 6.

$$dG=\frac{t\cdot ds}{2\rho_{ss}}+\frac{\Delta\cdot ds}{2\rho_{Cu}}=\frac{1}{2}\left(\frac{t}{\rho_{ss}}+\frac{\Delta}{\rho_{Cu}}\right)ds\ , \qquad (A5.3)$$

an expression for an elementary force acting on the screen contour region ds has a form:

$$dQ=B\cdot U\cdot dG=-x\left(\frac{t}{\rho_{ss}}+\frac{\Delta}{\rho_{Cu}}\right)B\frac{dB}{d\tau}ds\ . \qquad (A5.4)$$

(In expressions (A5.3) and (A5.4), ρ_{ss} and ρ_{Cu} are specific electric resistances of stainless steel and copper correspondingly and t and Δ are their thicknesses.)

Denoting a force normalization parameter

$$Q_0=-r^2\left(\frac{t}{\rho_{ss}}+\frac{\Delta}{\rho_{Cu}}\right)B\frac{dB}{d\tau}\ ,\ N/m, \qquad (A5.5)$$

we get (A5.4) in a more simple form:

$$dQ=Q_0\frac{x}{r^2}ds,\ N/m. \qquad (A5.6)$$

Addressing now to a real beam screen geometry (fig.2), we see that for a region between sections "a-a" and "b-b"

$$x=r\cdot Sin\alpha,\ ds=r\cdot d\alpha$$

and hence,

$$dQ(a,b)=Q_0 Sin\alpha\cdot d\alpha. \qquad (A5.6')$$

Analogously, it is easy to get

$$dQ(b,d)=Q_0\left(\frac{R}{r}\right)^2\left[\left(1+\frac{B}{R}\right)\frac{\sqrt{2}}{2}-Cos\beta\right]d\beta \qquad (A5.6'')$$

and

$$dQ(d,e)=Q_0\left[\frac{A}{r}-1+Cos(\gamma_0-\gamma)\right]d\gamma. \qquad (A5.6''')$$

Integrating these dependencies, one can find expressions for total horizontal forces in any point of every contour region:

$$Q(a,b)=Q_0(1-Cos\alpha),\ N/m, \qquad (A5.7)$$

$$Q(b,d)=Q_0\left(\frac{R}{r}\right)^2\left[\left(1+\frac{B}{R}\right)\frac{\sqrt{2}}{2}(\beta-\beta_0)-Sin\beta+Sin\beta_0\right],\ N/m, \qquad (A5.8)$$

$$Q(d,e)=Q_0\left[\left(\frac{A}{r}-1\right)\gamma+Sin\gamma_0-Sin(\gamma_0-\gamma)\right],\ N/m. \qquad (A5.9)$$

Considering instead of the whole beam screen contour only its quarter, one should apply force factors substituting an influence of dropped regions - a force A_a and moments M_a and M_e (fig.2).

The force A_a can be determined as a sum of all forces dQ along the contour between the sections "a-a" and "e-e":

$$A_a=\int_s dQ(s). \qquad (A5.10)$$

The moment M_a is determined by the theorem of Castigliano, according to which an angular displacement of a point "a" is equal to a derivative of a deformation energy of a considered contour region with respect to the moment M_a. Taking into account that the angular displacement in the point "a" must be nil because of contour symmetry, we get [8]:

$$\varphi_a=\frac{dU}{dM_a}=\frac{d}{dM_a}\left[\int_s\frac{M^2(s)ds}{2EJ}\right]=\frac{1}{EJ}\int_s M(s)\frac{dM(s)}{dM_a}ds=0,$$

or, as $\frac{dM(s)}{dM_a}=1$:

$$\varphi_a=\frac{1}{EJ}\int_s M(s)ds=0\ . \qquad (A5.11)$$

In latter expressions E is the elastic modulus and J - the inertia moment of the steel screen wall cross section (neglecting a small influence of thin copper coating).

Expressions (A5.10) and (A5.11) allow to find the force A_a and statically indefinable bending moment M_a, which appear to be in our case

$A_a \simeq 5.436\ Q_0$, N/m and $M_a \simeq 43 \cdot 10^{-3} Q_0$, Nm/m. (A5.12)

As to the value of the moment M_e, it is found now from the equilibrium analysis of the beam screen contour quarter under consideration and appears to be

$$M_e \simeq 30 \cdot 10^{-3}\ Q_0, \text{ Nm/m.} \qquad \text{(A5.13)}$$

Obtained results allow to find, in arbitrary screen point, the bending moment M and tensile force S (acting tangentially to the contour centre line in this point), and from them - the stress in screen material:

$$\sigma = \pm \frac{6M}{t^2} + \frac{S}{t}, \text{N/m}^2. \qquad \text{(A5.14)}$$

(In the latter expression a sign "+" before the first term refers to material fibres in tension, and "-" - to those in compression at screen bending; besides, the influence of the thin copper layer Δ is not accounted for.)

Notice that A_a, M_a and M_e (and, hence, M, S and σ) depend on Q_0, which in turn , via ρ_{ss} and ρ_{Cu}, depends on magnetic field value B, screen operating temperature T and copper coating thickness Δ - see A5.5.

Beam screen deformation calculation at quench is carried out also on the basis of the theorem of Castigliano. In this case dummy forces are applied sequentially to the screen - at first P1, stretching it horizontally, and then - P2, contracting it vertically. In both cases a derivative of the screen deformation energy with respect to the corresponding force produces a change of a given screen diameter. Resulting, for the horizontal screen diameter we have:

$$\delta_x = \frac{4}{EJ} \int_a^e M(s) \frac{dM(s)}{dP1} ds\ , \qquad \text{(A5.15)}$$

and for the vertical one -

$$\delta_y = \frac{4}{EJ} \int_a^e M(s) \frac{dM(s)}{dP2} ds\ . \qquad \text{(A5.16)}$$

For considered LHC beam screen these expressions give:

$$\delta_x \simeq 5.89 \cdot 10^{-7} Q_0, \text{ m} \qquad \text{(A5.15')}$$

$$\delta_y \simeq -5.94 \cdot 10^{-7} Q_0, \text{ m.} \qquad \text{(A5.16')}$$

Once again, as in the case with the stresses, the screen deformations are expressed via the normalization parameter Q_0, i. e. they vary with magnetic field, operating temperature and copper coating thickness. The maximal values of the parameter Q_0 (N/m) depending on the copper thickness Δ and operating temperature T at magnetic field varying between B=10 T and B=0 T are given in a tab.A5.1:

Table A5.1

Δ, μm	Operating temperature, K		
	20	50	70
20	1205	633	350
50	2940	1504	800
100	5832	2958	1547

By applying the expressions (A5.15') and (A5.16') and the data of the tab.5.1, it is easy to get the values of a horizontal screen diameter increase and vertical one decrease for different copper coating thicknesses and operating temperatures.

REFERENCES

1 "DESIGN STUDY OF LHC". - 02/05/91, CERN-91-03.

2. *A.Poncet.* "MEMORANDUM". - MT-ESH/AP, October 20, 1993.

3. Catalogue of high energy accelerators. HEACC'92. Hamburg, Nov.1992.

4. "BEAM SCREEN AND COLD BORE - DESIGN CHOICES". - CHAMONIX, VACUUM SESSION, 28.09.93.

5. "LHC - ACCELERATING PROJECT" - CERN/AC/93-03(LHC).

6. *S.Timoshenko, D.H. Young, W.Weaver.* "VIBRATION PROBLEMS IN ENGINEERING". - JOHN WILEY & SONS, New York, Chichester, Brisbane, Toronto, Singapore.

7. *Stephen P. Timoshenko, James M. Gere.* "MECHANICS OF MATERIALS". - VAN NOSTRAND REINHOLD COMPANY, New York, Cincinnati, Toronto, London, Melbourn. - 1972.

8. STRENGTH OF MATERIALS. - Part 1. - Elementary theory and problems. - By S. Timoshenko. - D.van Nostrand Company, INC. Prinseton, New Jersey.

9. *M.M.Karliner, N.V. Mityanina, V.P. Yakovlev.* "MULTIBUNCH RESISTIVE WALL INSTABNILITIES OF AN INTENSE ELECTRON BEAM IN STORAGE RINGS". Novosibirsk, 1992, preprint BINP 92-52.

10. *M.M.Karliner.* Preprint INP 74-105 (in russian).

11. *H.Bruck.* "ACCELERATEURS CIRCULAIRES DE PARTICULES". PRESSES UNIVERSITAIRES DE FRANCE, 1966.

12. *Chambers R.S.* The anomalous skin effect. Proc. Roy. Soc. A, 1952, 215, N 1123, p.481-496.

13. *Pippard A.B.* Metallic conduction at high frequencies and low temperatures. Adv. Electron., 1954, 6, p.1-45.

M.M. Karliner, N.V. Mityanina,
B.Z. Persov, V.P. Yakovlev

LHC Beam screen design analysis

М.М. Карлинер, Н.В. Митянина,
Б.З. Персов, В.П. Яковлев

Анализ проекта лайнера LHC

BudkerINP 94-45

Ответственный за выпуск С.Г. Попов
Работа поступила 10 мая 1994 г.

Сдано в набор 20.05. 1994 г.
Подписано в печать 30 мая 1994 г.
Формат бумаги 60×90 1/16 Объем 2,5 печ.л., 2,0 уч.-изд.л.
Тираж 220 экз. Бесплатно. Заказ N 45

Обработано на IBM PC и отпечатано на
ротапринте ИЯФ им. Г.И. Будкера СО РАН,
Новосибирск, 630090, пр. академика Лаврентьева, 11.